
Article:
Liu, H., Li, J., Shao, S. et al. (1 more author) (2015) SPH modeling of tidal bore scenarios. Natural Hazards, 75 (2). 1247 - 1270. ISSN 0921-030X

https://doi.org/10.1007/s11069-014-1374-2

SPH Modeling of Tidal Bore Scenarios

Huaxing Liu[1], Jing Li[2], Songdong Shao[3] and Soon Keat Tan[4]
[1] Maritime Research Centre, School of Civil and Environmental Engineering, Nanyang Technological University, Singapore, Email: liuhuaxing@ntu.edu.sg (Author of correspondence)
[2] Deepwater Technology Centre, Det Norske Veritas, Singapore, Email: jing.li@dnvgl.com
[3] Department of Civil and Structural Engineering, University of Sheffield, Sheffield, United Kingdom (State Key Laboratory of Hydro-Science and Engineering, Tsinghua University, Beijing, China), Email: s.shao@sheffield.ac.uk
[4] Maritime Research Centre, School of Civil and Environmental Engineering, Nanyang Technological University, Singapore (Nanyang Environment and Water Research Institute NEWRI, Nanyang Technological University, Singapore), Email: ctansk@ntu.edu.sg

ABSTRACT

The paper presented a Smoothed Particle Hydrodynamics (SPH) method to study the three-dimensional (3D) tidal bore scenarios. The SPH method is a mesh free particle modeling technique that can track the large deformation of free surfaces in a straightforward and accurate way. Two benchmark cases of the tidal bore propagation were computed and compared with the experimental results. The first one is related to the undular and breaking bores in a regular open channel and the second one considers the undular bore passing through the contraction of bridge piers. Physical laboratory experiments have also been carried out to validate the numerical investigations. The comparisons of both the free-surface profile and velocity field demonstrated that the SPH technique could provide a very promising tool to simulate tidal bore phenomena in engineering practice. The work is the first to systematically explore the potentials of mesh-free SPH modeling approach in predicting the tidal bore features under 3D flow conditions.

Key Words: tidal bore, SPH, domain separation, undular bore, breaking bore, bridge pier contraction

1. Introduction

When a river mouth has a flat converging funnel shape and large tidal range (typically more than 6 m), a typical tidal bore can be observed during the spring tide. A tidal bore is a wave or a series of waves propagating upstream as the tidal flow turns to rising. Tidal bores constitute one of the most energetic events in an estuary system. When a bore approaches, a giant wall of the water comes hurtling with a powerful roar, usually creating a unique natural landscape of local spot. However, the large fluid velocity at the bore front and the associated turbulence can often cause significant erosions and scouring on the riverbed, and threaten to erode the foundation of hydraulic structures. Therefore, a comprehensive knowledge and modeling of the tidal bore process is of significant importance in the hydraulic engineering, in terms of the river bank protection and sediment load transport.

Although the tidal bore phenomenon has been studied for centuries, it is still poorly understood due to the complexity involved. Field investigations are quite limited because the large impact force of the bore flows often caused the malfunction and failure of scientific equipments (e.g. Simpson et al., 2004). Even in some successful measurements, the recorded data were all based on the fixed-point measurements, and such a data set was limited and not accurate enough to describe such a dynamic flow process that extends over kilometers of distance. Many laboratory experiments have also been conducted on the study of formation and propagation of the tidal bores (e.g. Benet and Cunge, 1971; Treske, 1994), as well as the influence of hydraulic structures on the bore propagation, such as a river gate (Zhu and Cheng, 2008) or bridge piers (Chanson, 2011). Also due to the limitation of the measuring techniques and instrumentations, most of these studies were based on the visual observations, or simply the free-surface profiles. Recent interests in the experimental analysis have concentrated on the detailed flow field characteristics beneath the bore front (Hornung et al., 1995).

On the other hand, numerical simulations can provide an effective way to study the bore phenomenon. The Shallow Water Equations (SWEs) have been extensively used, discretized by an appropriate numerical scheme, such as the Finite Element Method

(Morrison, 2008), Finite Difference Method (Madsen et al., 2005; Liang et al. 2006) and Finite Volume Method (Su et al., 2001; Pan et al., 2007; Pan and Huang, 2010). The SWEs assumes a constant velocity field throughout the fluid depth, by which the 3D Navier-Stokes Equations reduce to 2D horizontally. Thus it can deal with a large scale simulation comprising of the tidal bore generation and propagation, but the violent velocity structures at the bore front can be smoothed as well. Recently, Furayama and Chanson (2010) presented the simulations of bore flow in a uniform channel by solving the Navier-Stokes Equations with the Cubic-Interpolated Pseudo-particle Combined Unified Procedure (CIP-CUP) method equipped with a Large Eddy Simulation turbulence model. Also the Reynolds-Averaged Navier-Stokes (RANS) model has been used by Lin and Liu (1998) for some more complex tidal wave simulations. However, these numerical works were all based on the Eulerian grid that spans the whole computational domain, thus additional techniques have to be required to capture the free surface movement, such as the Volume of Fluid (Hirt and Nichols, 1981). Besides, these grid-based methods are sometimes relatively time-consuming due to the dynamic re-meshing, and they also suffer numerical diffusions especially in the large deformation of free surfaces. Here it is worth mentioning that more practically oriented simulation works in the tidal bore field have been documented by Chen et al. (2005), Zheng et al. (2008) and Behera et al. (2011).

A relatively new numerical method that shows great potential in the simulation of violent fluid flows is the mesh-free Smoothed Particle Hydrodynamics (SPH), a gridless method that originated in the astronomical application (Lucy, 1977; Gingold and Monaghan, 1977) and was later applied to a variety of free surface flows (Monaghan, 1994). SPH is based on the concept of representing the continuous fluid with a finite set of discrete particles, whose interactions and movements are prescribed by the Navier-Stokes equations. By adopting a Lagrangian frame of reference, the mesh is not needed in the SPH framework. This makes SPH circumvent many of the issues related to the grid-based models, such as the numerical diffusions resulted from the mesh distortion and the additional CPU overheads caused by the mesh re-generation and interface tracking. This is especially true when the large deformation or fragmentation of the free surfaces is involved, such as that around the bore front area. Motivated by the interesting but unclear features of the tidal bore

phenomenon, as well as the possible prospect of the SPH applications in related field, the present research applies the SPH concept to the tidal bore simulations. Until now, two distinct versions of the SPH modeling techniques have been used, i.e. the Weakly Compressible SPH (WCSPH) and the Incompressible SPH (ISPH) approaches. The former solves the fluid pressure field by using an explicit equation of state, while the latter semi-implicitly solves a pressure Poisson equation based on either the velocity divergence free or particle density invariant criterion. Although both SPH methods have the pros and cons, the WCSPH seems to be more efficient in CPU expense when dealing with a huge number of the fluid particles in a practical 3D simulation, as its numerical scheme is fully explicit and there is no need to construct a large sparse matrix to solve the linear equation. Thus in the present work, we use the WCSPH as a basic numerical tool for the proposed tidal bore studies. Another purpose of the study is to evaluate the potential applications of SPH modeling technique in a practical field. Although the SPH modeling approach has been used to quite a few benchmark cases in the laboratory scale, its applicability in an engineering scenario is yet to be fully investigated. Recent good work to use SPH for Tsunami wave breaking simulation was reported by Xie et al. (2012) based on a corrected 3D SPH numerical scheme.

The SPH concept has already been used for the tidal bore applications in terms of the 2D form, for instance, Monaghan (1994), Bonet and Lok (1999) and Landrini et al. (2007). However, most of these studies tended to use the tidal bore only as one benchmark test for the follow-on model applications. There have been limited systematic works dedicated to the SPH application in this field. The most recent work of St-Germain et al. (2014) pioneered the SPH to investigate hydrodynamic forces generated by a rapidly advancing hydraulic bore and also Farahani et al. (2014) applied the 3D SPH modeling concept for a bar/rip channel system. However, 3D bore characteristics are scarcely revealed, which is definitely an important forte of the SPH. The 3D propagation of bore flows in both an open flume and through the bridge piers was tentatively investigated by the authors (Liu et al., 2010; Li et al., 2010) in a previous conference proceeding work. As a continuation and enrichment, the present paper systematically studies the undular and breaking bore propagation and the undular bore passing through the bridge pier contraction, aiming to disclose the fundamental differences in the bore flow features. An effective domain separation

treatment has been proposed in the SPH numerical scheme to reduce the CPU cost in 3D simulations. Besides, relevant laboratory experiments have been conducted for the two tidal bore situations to validate the numerical works.

2. SPH Methodology

The main features of the SPH model adopted in the present research are summarized as below. More detailed descriptions can be found in the following references (Monaghan, 1992; Liu and Liu, 2003).

2.1 Basic SPH Equations

Consider a set of particles distributed over the computational domain, in which each one carries the specified fluid properties such as the mass m, density ρ, pressure p, position $\mathbf{r}$ and velocity $\mathbf{v}$. For a given particle a, it moves in the force field generated by the entire particle system and its physical fluid properties evolve according to certain evolution laws, i.e. Euler equations for a compressible Newtonian fluid. The interpolated mass and momentum equations in SPH are written as

$$\frac{d\rho_a}{dt} = \rho_a \sum_b \frac{m_b}{\rho_b} \mathbf{v}_{ab} \cdot \nabla_a W_{ab} \tag{1}$$

$$\frac{d\mathbf{v}_a}{dt} = -\sum_b m_b \left(\frac{p_a}{\rho_a^2} + \frac{p_b}{\rho_b^2} + \Pi_{ab} \right) \nabla_a W_{ab} + \mathbf{g} \tag{2}$$

where the summation is over all the particles, one of which is particle b. ρ is the density, t is the time, m is the particle mass, P is the pressure, $\mathbf{v}_{ab} = \mathbf{v}_a - \mathbf{v}_b$ is the velocity difference, $\mathbf{g}$ is the gravitational acceleration vector, W_{ab} is the contribution of particle b to the kernel function W at particle a and ∇_a denotes the gradient taken with respect to the coordinates of particle a. Besides, Π_{ab} is

defined as an artificial viscosity to ensure the numerical stability (Monaghan, 1992).

To close the governing equations, an Equation of State (EOS) should be used in the SPH to acquire the pressure field. The most frequently used EOS for water is the so-called Tait equation as below

$$\mathrm{p} = \mathrm{B}[(\frac{\rho}{\rho_0})^{\gamma} - 1] \tag{3}$$

where $\gamma = 7$, $\mathrm{B} = \mathrm{c}_0^2 \rho_0 / \gamma$ with $\rho_0 = 1000.0 \mathrm{kg/m}^3$ being the reference density for water and c_0 being the corresponding sound speed. By using the above EOS, the fluid pressures can be solved explicitly. This is very straightforward to program and thus the WCSPH performs more or less faster than the ISPH that solves a pressure-velocity coupled equation, such as the Poisson equation at each time step. In the WCSPH, however, the fluid is treated as weakly compressible, so a limitation of sound speed (about ten times faster than the maximum fluid velocity) must be imposed to keep the density variations small enough for the conservation of fluid volume.

The position change of a particle can be predicted by the following equation of motion

$$\frac{\mathrm{d}\mathbf{r}_\mathrm{a}}{\mathrm{dt}} = \mathbf{v}_\mathrm{a} + \varepsilon \sum_\mathrm{b} \mathrm{m}_\mathrm{b} \frac{\mathbf{v}_\mathrm{ba}}{\rho_\mathrm{ab}} \mathrm{W}_\mathrm{ab} \tag{4}$$

where the weighting parameter ε takes the value of 0.5. Instead of using $\mathrm{d}\mathbf{r}_\mathrm{a} / \mathrm{dt} = \mathbf{v}_\mathrm{a}$, herein the particle moves with a modified velocity that is closer to the average velocity of the neighboring particles. This variant reduces the particle disorder and smoothes out the oscillations in the pressure field. However, a slight change in the density field can be magnified by the EOS, which leads to physically unrealistic flow behaviors at the free surface. This situation can be efficiently overcome by reinitializing the density field with a first-order interpolation scheme that is performed periodically over the fluid domain. In the present SPH computations, an MLS filter is used to reinitialize the density field at a frequency of every 30 time steps to achieve the optimum model performance.

To treat the flow turbulence during the tidal bore propagation and breaking, the turbulent force must be added to Eq. (2) to account for the turbulence generation and damping. Here a simple and effective eddy viscosity based Sub-Particle Scale (SPS) turbulence model originally developed by Gotoh et al. (2001) is used

$$\tau_{ij} / \rho = 2\nu_T S_{ij} - \frac{2}{3} k\delta_{ij} \tag{5}$$

where ν_T is the turbulence eddy viscosity, S_{ij} is the strain rate of mean flow, k is the turbulence kinetic energy, and δ_{ij} is the Kronecker's delta. As for the turbulence eddy viscosity ν_T, the Smagorinsky model is adopted as follows

$$\nu_T = (C_s \Delta X)^2 |S| \tag{6}$$

where C_s is the Smagorinsky constant, ΔX is the particle spacing, which represents the characteristic length scale of small eddies, and $|S| = (2S_{ij} S_{ij})^{1/2}$ is the local strain rate.

2.2 Solid Boundary Condition

When the fluid particles approach the solid boundaries, like the bottom or side walls of a numerical wave flume, the lack of particles outside the boundaries presents incomplete support to the nearby particles. This deficiency leads to a density decrease of relevant particles and unrealistic numerical solutions. To overcome this problem, the solid boundary is usually discretized as the virtual particles which can produce repulsive forces to the particles close to the physical boundary, either actively or passively. In an active force scheme (Monaghan, 1994), one layer of particles is placed right on the boundary line, and it exerts central forces to the approaching particles that fall inside their compact support regime. While in the passive force approach, several layers of virtual particles are assigned on and outside the boundary line to provide compact support for the neighboring fluid particles. These virtual particles are subject to the same governing equations as the inner fluid particles, so their densities increase when the other fluid particles are approaching, and the same is

true with the pressure. Repulsive forces generated due to the pressure gradient are then used to update the inner fluid particle positions to prevent their penetration. However, the movement of these virtual particles is not determined by Eq. (4). They could remain either fixed at their initial positions (Shao and Lo, 2003; Crespo et al., 2007), or move with the velocity extrapolated from the inner fluid particles (Cummins and Rudman, 1999). In this paper, the solid boundaries are treated by following Shao and Lo (2003).

2.3 Inflow Boundary Condition

For the numerical simulations of tidal bore propagation carried out in the following sections, a unidirectional steady inflow condition is needed. Some advanced inflow boundary works in the particle methods have been developed, such as in Gotoh et al. (2001) and Lastiwka et al. (2009), in which an inflow zone was defined outside the flow domain and once a particle crosses from the inflow zone into the fluid domain, it turns into a fluid particle and meanwhile, a new particle enters the inflow zone from the other side of the domain. In our computations, it has been found that in order to maintain a stable longtime bore propagation, a moving solid wall method is more efficient to generate such an inflow condition. To implement this, we just simply push a solid impermeable vertical wall at one end of the channel flume with an adequate speed so as to achieve the required tidal bore velocity. This method is not only simple to program but also can effectively avoid the possible numerical instabilities arising from the fluctuation of fluid particles near the inflow zone. Naturally, it is inevitable that some kinds of the small disturbance wave can be generated on the free water surface, but this should not produce a negative influence on the computations, as long as we take the numerical results well before these disturbances get into the simulated region of interest.

2.4 Domain separation procedure

When the physical geometry and flow patterns are symmetrical with respect to a certain plane, a simple domain separation algorithm can save considerable computational efforts. As far as the present knowledge is concerned, very limited

works have been reported in this aspect for a 3D SPH simulation. In this paper, the computational domain is separated along the symmetric line by creating a series of ghost particles near the symmetric plane, as depicted in Fig. 1. For each fluid particle close to the symmetry plane (grey solid circle), a mirror particle is automatically generated (hollow circle). The mirror particle shares the same properties as its prototype except that it has the opposite normal velocity. The thickness of the mirror particle layer is chosen to satisfy the compact support of nearby fluid particles, i.e. not less than $2h$. This mirroring procedure is performed at each time step to ensure a zero flux across the symmetrical plane. The employment of such a domain separation procedure can greatly reduce the computational overhead. With the particle number N halved, the number of interactions per time step and, consequently, the computational time diminishes logarithmically as per $N \log N$, given that the linked-list particle searching algorithm (Monaghan and Lattanzio, 1985) is implemented. It has been found from the computations that the CPU load reduced by roughly 50% and the effect was more prominent when more particles were used.

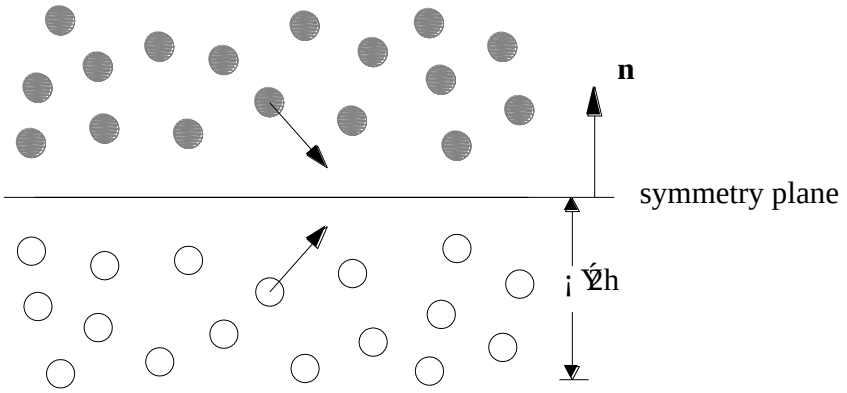

Fig. 1 Illustration of domain separation by using symmetry plane

Here it should be noted that this method will not work in a 3D application in which the lateral variations of fluid properties are large, such as that in a violent 3D wave breaking situation. However, this method is expected to work well for quite a few 3D flow applications with symmetry property in the cross-sectional directions. Also it

should be realized that this domain separation technique is different from the traditional symmetric boundary treatment widely used in other SPH algorithms, as the latter is often used to deal with the solid boundary or free surface, while in this work we improved this treatment for the inner flow domain separation aiming to reduce the CPU load.

3. Undular and Breaking Bore Flows in an Unconfined Open Channel

The undular and breaking bores are quite different in their flow features and energy transfers, especially for a mobile bed situation. In a recent pioneering work, Khezri and Chanson (2012) found that in the undular bore experiment, the sediment movement was almost negligible, while some strong sediment motions were observed beneath the breaking bore. In a practical field, this can have a major impact on the sediment processes in the estuarine zone. Thus in this section we will use both the laboratory experiments and numerical SPH simulations to investigate these two types of tidal bore and examine their free surface profiles and velocity structures.

3.1 Laboratory Bore Flume and Measurement Results

The undular and breaking bore generations and propagations were studied in the laboratory tests. The experimental bore flume and measurement facilities are shown in Fig. 2. The tests were performed in a 6 m long re-circulating open channel located in the Maritime Research Centre, Nanyang Technological University. The test section has a rectangular cross-section of 0.3 m in width and 0.4 m in height. Uniform inflows with any desirable surface velocity between 0.02 m/s and 0.7 m/s could be generated by a centrifugal pump fitted with a variable speed controller. A fast closing sluice gate was installed at the other end of the channel, the sudden closure of which could generate a bore flow propagating upstream. The initial water depth was fixed at 0.1 m during the experiment. The initial flow velocities of 0.3 m/s and 0.7 m/s were produced respectively, to generate the conditions of undular and breaking bore propagations, with the corresponding Froude number of 1.19 and 1.63. For each velocity, 5 runs were carried out to ensure the repeatability.

The flow scenarios were recorded non-intrusively by a Particle Image Velocimetry (PIV) system through the glass walls at bottom and sides. A double cavity Nd:YAG laser (power ~130 mJ per pulse, duration ~ 5ns) was employed to illuminate the flow field. A 12-bit charge-coupled device (CCD) camera was used to acquire the images at a frame rate of 15 Hz, and a resolution of 1600×1200 pixels. The viewing area was chosen at 300 mm × 200 mm. In the post-processing stage, the surface elevation at a given location as well as the velocity fields was extracted frame by frame.

Fig. 2 Laboratory bore flume and measurement facility

The typical snapshots of the free surface and velocity structure recorded in the laboratory experiment are shown in Fig. 3 and Fig. 4, respectively, for the initial velocity of 0.3 m/s and 0.7 m/s, corresponding to the undular and breaking tidal bores. It is shown that the front of an undular bore assumes a very smooth shape followed by a train of well-defined undulations. In comparison, the breaking bore has a very distinct two-dimensional roller region similar to that observed in a coastal wave breaking with fragmented water surfaces and high energy concentrations, which is characterized by the production of large-scale turbulences and vortices. Some previous studies have investigated similar unsteady turbulences induced by the breaking tidal bore and it has been highlighted that the intensive mixing processes

exist beneath the bore front. This is also clearly demonstrated by the present experimental findings.

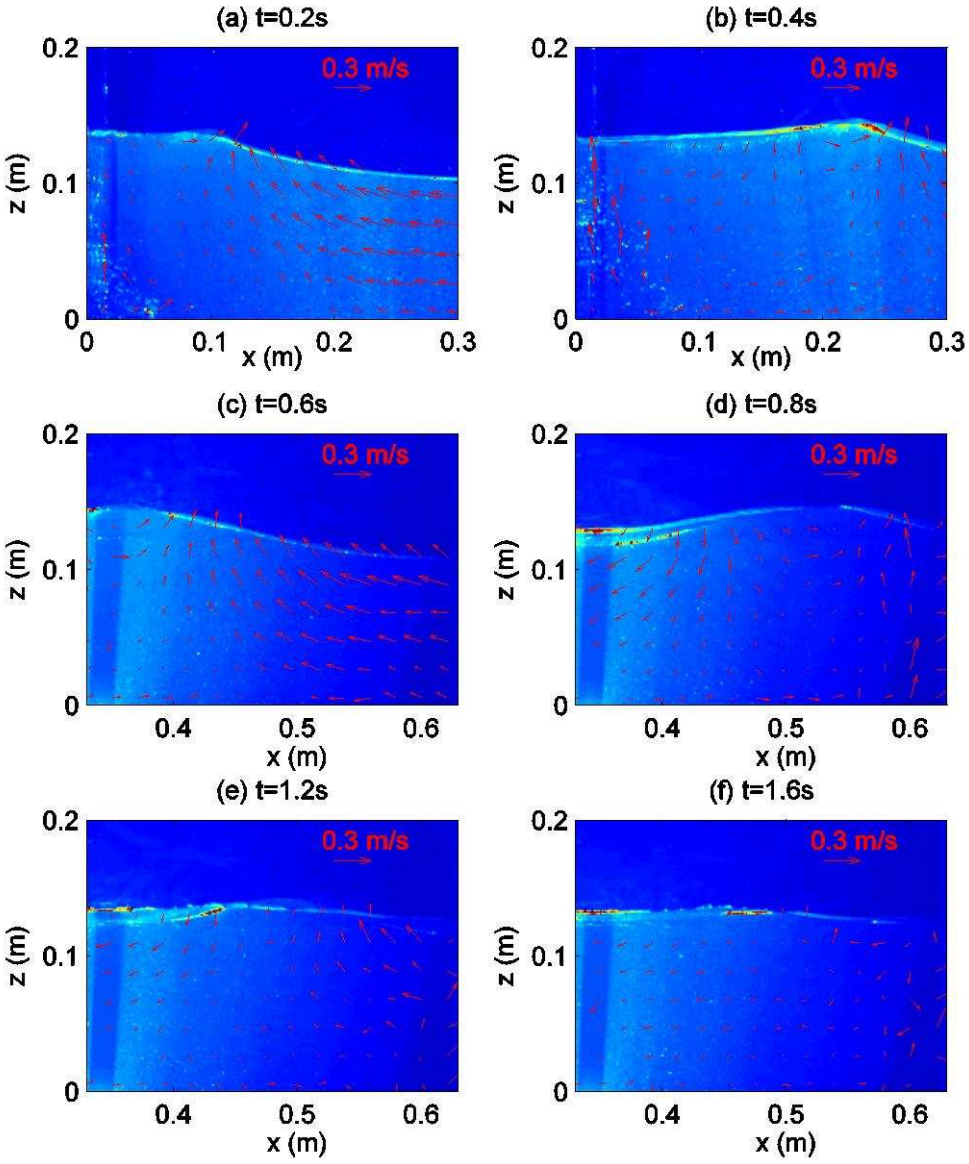

Fig. 3 Experimental images of undular bore and associated velocity fields

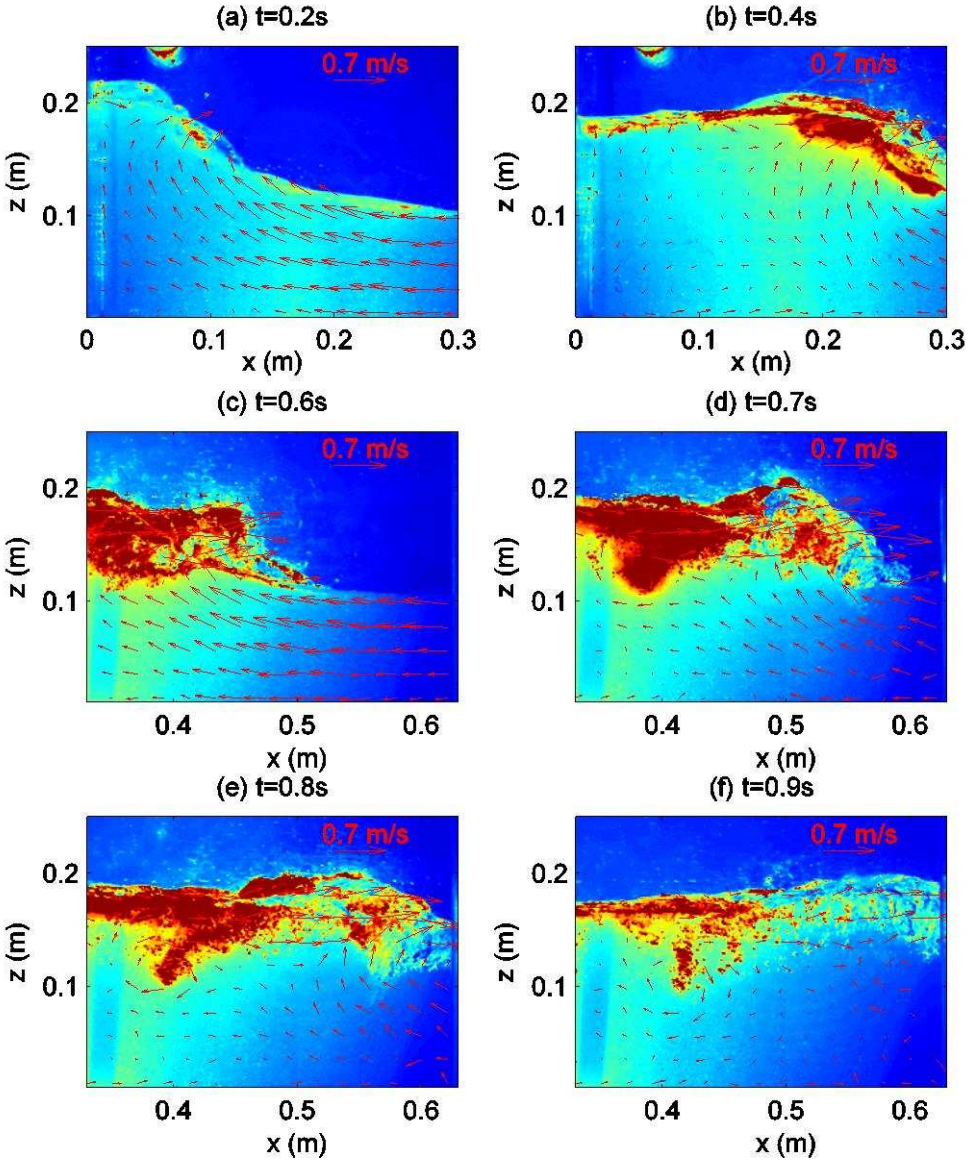

Fig. 4 Experimental images of breaking bore and associated velocity fields

3.2 SPH Simulations of Undular and Breaking Bores

In this section, the proposed SPH model is used to reproduce the physical experiment of two tidal bore flows. The numerical model code is modified from the open source code SPHysics (Gómez-Gesteira et al., 2012). To reduce the computational cost, the numerical open channel flume is taken as 3 m long, 0.3 m wide and 0.4 m high. Following the experimental setting, the initial water depth is 0.1 m and initial flow velocity of 0.3 m/s and 0.7 m/s are used. At the beginning of computation, the fluid particles are originally distributed with a uniform particle spacing of 0.005 m on a lattice coordinate. Only half of the numerical flume is involved in the simulations by adopting the domain separation treatment as described above. Thus a total number of 580,752 particles are used based on this configuration, including 212,634 fixed boundary particles for the channel fixed wall and 8,118 moving boundary particles for the inlet flow wall. A predictor-corrector scheme as described in Monaghan (1994) is used with a time step $\Delta t = 2.0 \times 10^{-5}$ s. The numerical simulations are carried out until time $t = 1.6$ s for the whole bore propagation process.

From the SPH simulations, Fig. 5 shows the generation and propagation of an undular tidal bore with the initial velocity of 0.3 m/s. As the inflow hits on the vertical end wall, the water surges up with a drastic water level increase ($t = 0.2$ s). This positive surge then propagates upstream in the form of a wave front ($t = 0.4$ s). The second bore wave front emerges at time $t = 0.6$ s and starts to propagate at $t = 0.8$ s as the inflow continuously gets into the channel flume. Finally the undular shaped bore is well established with a smooth rise of the free surface followed by a train of well-formed stationary waves, as shown at $t = 1.6$ s.

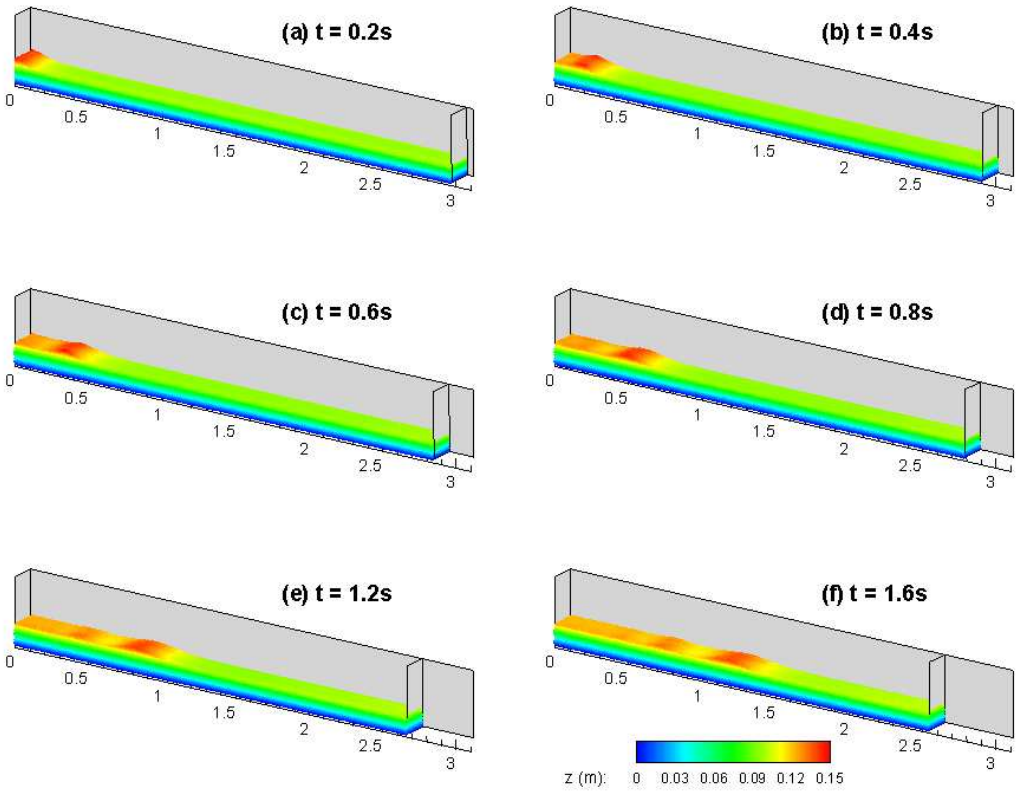

Fig. 5 SPH simulations of free surface profiles for an undular bore

With an initial flow velocity of 0.7 m/s (as shown in Fig. 6), the water surges up at the end wall with a more rapid water level rise, and then it curls and splashes down with high speed such like a dam break wave impacting on the solid wall. Apparently, the front of the bore evolves into a breaking wave and the existence of 2D roller region is clearly demonstrated. Then the bore propagates towards the upstream side of the computational domain and gradually dies out as the bore breaking process along the channel dissipates out most of the flow energy. During the whole bore generation and propagation process, the features of water splash up, overturning and breaking are clearly disclosed by the SPH computations. Compared with the previous undular bore, the present breaking bore is much more violent, involving significant free surface deformations and fragmentations.

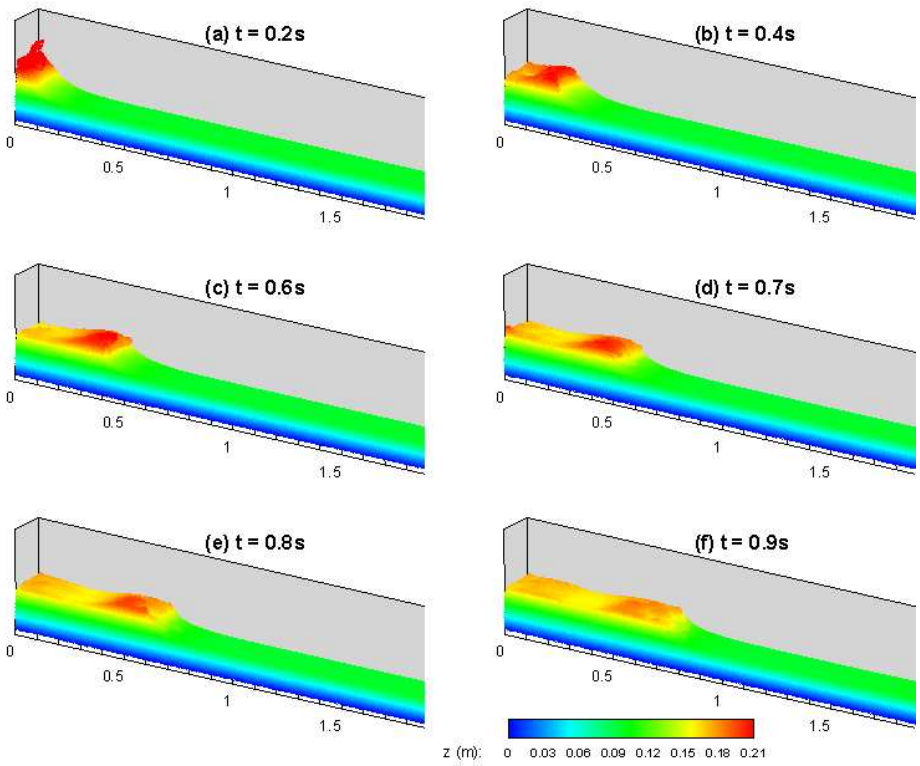

Fig. 6 SPH simulations of free surface profiles for a breaking bore

To quantitatively validate the numerical SPH simulations, the comparisons of time history of free surface profiles at three different locations along the channel flume are made with the experimental measurements, as shown in Fig. 7 and Fig. 8, respectively, for the undular and breaking tidal bores. The computational results showed an overall good agreement with the experimental observations in both the water surface amplitude and the bore front arrival time. Clearly an abrupt surge of the water level is observed when the leading bore wave front passes by, which is followed by a series of waves with the smaller amplitude. This has been demonstrated in both the numerical and experimental data. The data agreement in the breaking bore case in Fig. 8 is less satisfactory as compared with the undular bore in Fig. 7, which is attributed to the measurement difficulties in capturing the exact water surface due to the free surface fragmentations and aerations. Besides, the SPH particles are much more disordered when the surface breaking happens, leading to slightly larger numerical discrepancies. Generally speaking, the averaged error was found to be 0.72% in the undular bore and 2.08% in the breaking bore.

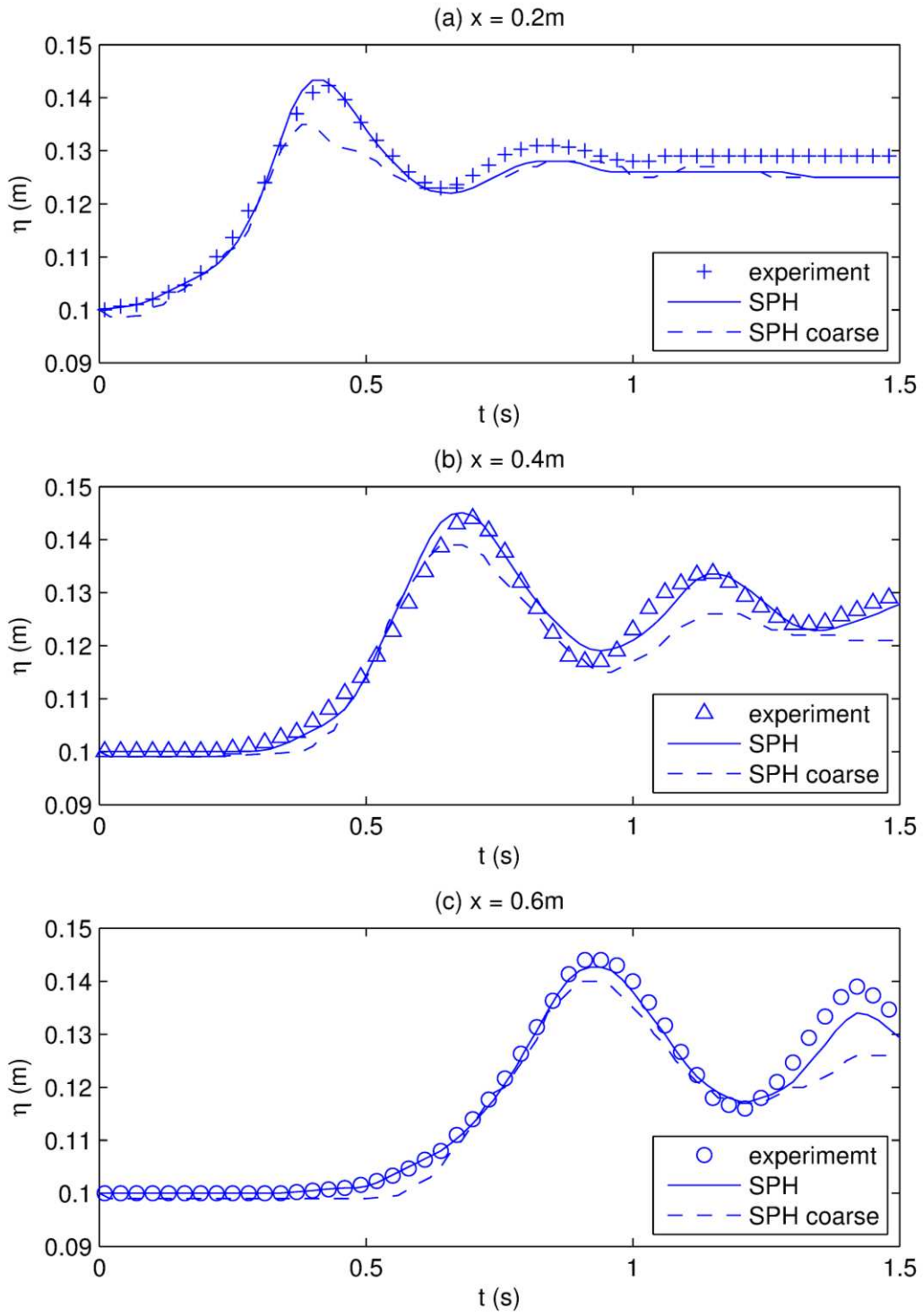

Fig. 7 Comparisons between two computed and measured free surface profiles at different locations for an undular bore

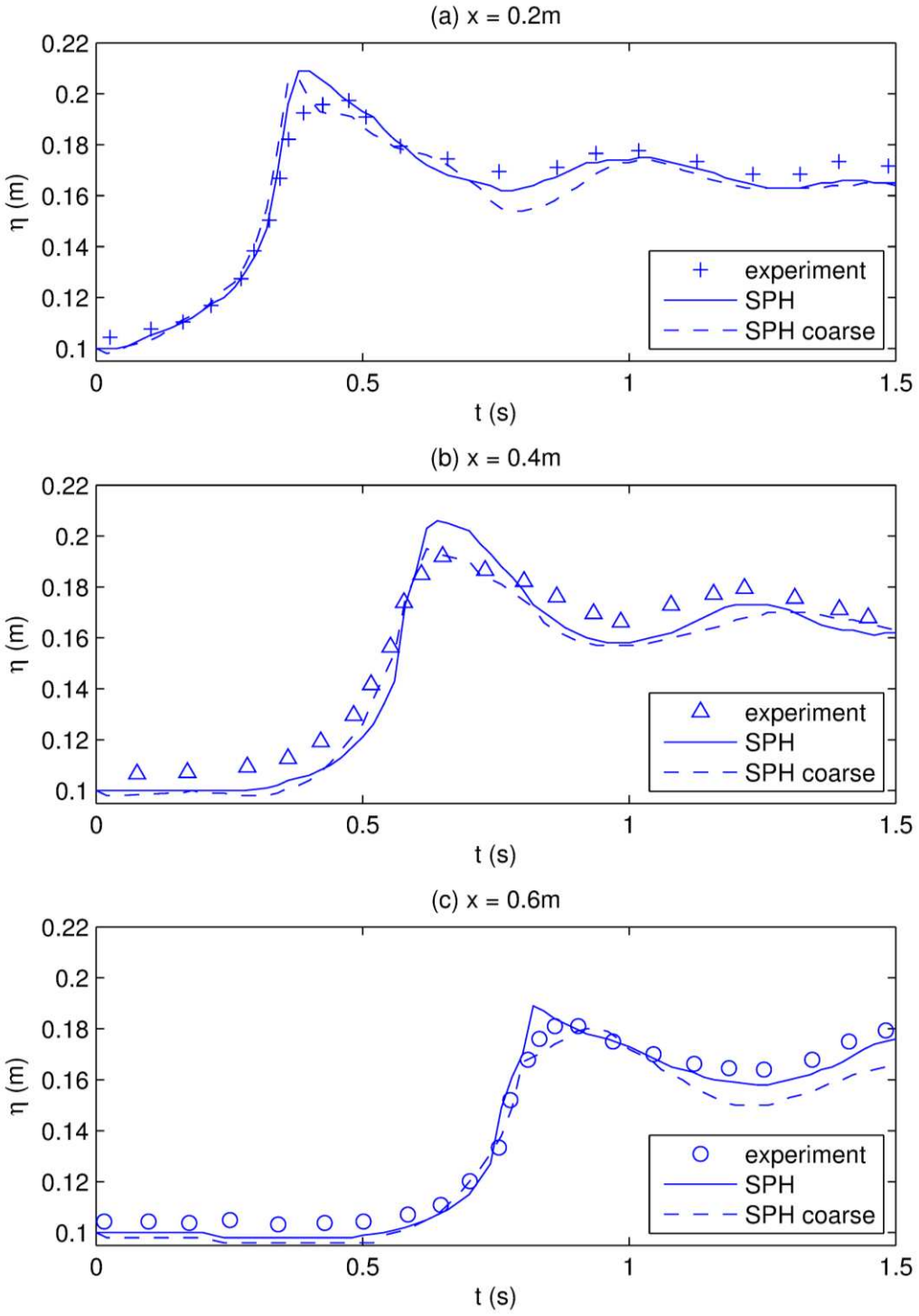

Fig. 8 Comparisons between two computed and measured free surface profiles at different locations for a breaking bore

To evaluate the sensitivity of the model, the comparisons of numerical results using different initial particle spacing are also shown in the above two figures. The model has employed a relatively coarser particle spacing of 0.01 m, as further refining this would be more CPU expensive. Although the coarse model simulations show some discrepancies near the measured peak points, the general agreement is acceptable in view that the two curves demonstrate a similar trend. By balancing both the model accuracy and computational overhead, the present computational particle spacing of 0.005 m should be deemed to be adequate.

The SPH computed flow velocity fields are shown in Fig. 9 and Fig. 10, respectively, for the undular and breaking bores. It is shown that the simulated flow patterns and velocity structures are very similar to those found in the laboratory experiments as shown in Fig. 3 and Fig. 4, in that the propagation of an undular bore is a mild flow evolution process, in which the velocity field keeps a quasi-symmetric non-breaking wave pattern. In comparison, the propagation of a breaking bore is a much more violent process in which the velocity magnitude is twice more larger. Besides, very large velocity components and gradients concentrate near the bore front. For example, between time $t = 0.4$ s and $t = 0.8$ s in Fig. 10, the bore severely breaks and the broken bore propagates in the nearly horizontal direction. Thus the breaking bore behavior is more or less like a typical costal wave breaking simulated in many SPH applications. Due to the large velocity variations, it can be concluded that the turbulence generation and fluid particle mixing are also much more intensive in the breaking bore, as compared with the undular bore. This phenomenon has been experimentally disclosed by Khezri and Chanson (2012). In general, the SPH computations satisfactorily demonstrated both types of the tidal bore velocity structures and this is due to the fact that the mesh-free SPH approach has the capability of treating the free surfaces of large deformation without the numerical diffusion and thus can realistically reproduce these violent flows.

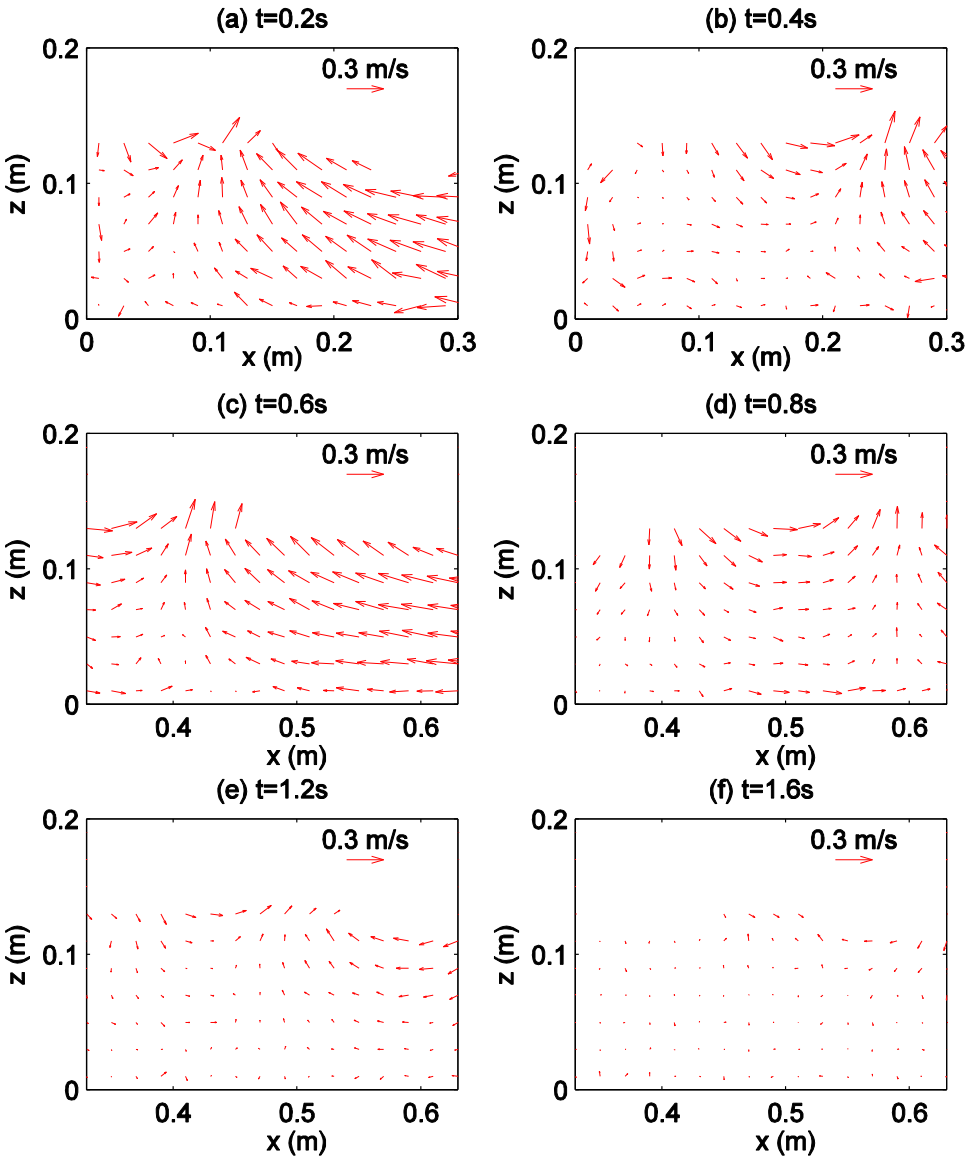

Fig. 9 SPH computed flow velocity fields for an undular bore

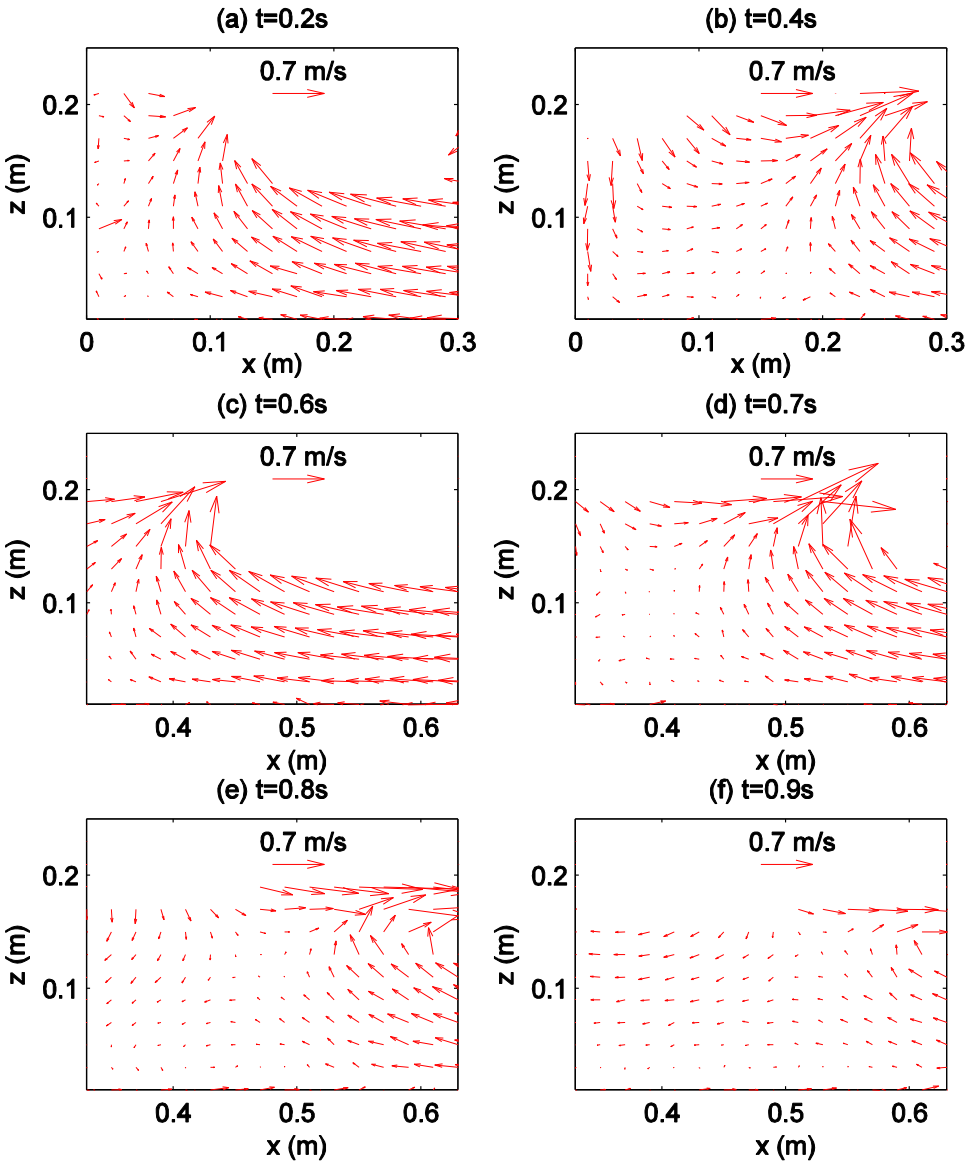

Fig. 10 SPH computed flow velocity fields for a breaking bore

4. Undular Bore Passing through Confined Bridge Piers

The presence of bridge pier constrictions can have a major impact on the free surface and turbulent mixing properties as well as flow potential energy when a tidal bore passes through. The tidal bore will demonstrate a totally different behavior as compared with the same bore in a channel without any constrictions. According to Chanson (2011), the impact of a tidal bore on the bridge pier as well as the effect of bridge pier on the tidal bore process have not been widely documented, although some limited progresses have been made in some field observations. Thus here we will use both the laboratory experiment and proposed 3D SPH simulations to investigate such a problem.

4.1 Laboratory Experiment and Recordings

The laboratory experiment to study the constriction effect of bridge piers on the undular bore propagation was also conducted in the same open channel flume used in the previous section. The experimental configurations followed Chanson (2011) in the general layout, but here we adopted a slightly different model dimension due to the space limitation and manufacturing issue, which is shown in Fig. 11.

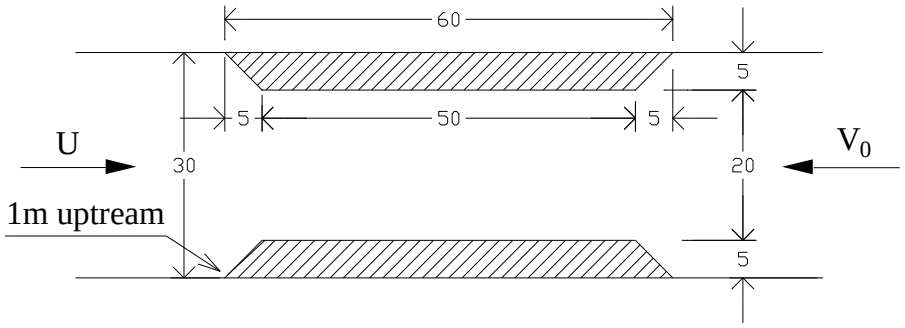

Fig. 11 Sketch of pier setup in an undular bore channel (Unit: cm)

In the above flume, the two half-channel constrictions which represent the bridge piers across a river are located 1.0 m upstream of the gate position. The convergent

sections have a slope of 1:1 and the water depth was initially set at 0.1 m. The flow arriving from the upstream with an initial velocity 0.3 m/s was blocked by the sluice gate and thus the resulting tidal bore flow traveled upstream subsequently. The PIV system was employed both horizontally (at z = 0.05 m) and vertically (at symmetry plane) to record the bore propagations, and the time histories of free surface were extracted at the locations of x = 1.0 m, 1.4 m and 1.6 m, respectively, corresponding to the entrance, mid-section and exit of the pier location. The pier model used in the experiment and one tidal bore observation photo are shown in Fig. 12.

Fig. 12 Experimental photo of tidal bore passing through channel constrictions

The observed flow patterns have been found to be similar to the experiment reported in Chanson (2011). Both experimental visual observations have showed that the entrance of the converging constrictions was associated with some reflecting bores propagating towards the channel downstream end, together with the development of a highly turbulent free surface inside the contractions, where the free surface exhibited some strong three-dimensional patterns. However, after the tidal bore has exited the channel constrictions, it reverted to its original quasi two-dimensional appearance again. This process indicated that the existence of the channel constrictions greatly changed the tidal bore hydrodynamics.

Fig. 13 and Fig. 14 are the PIV recorded images and associated velocity fields both horizontally and vertically. The times correspond to when the bore front just arrives at the entrance, and propagates in the contraction region, respectively. Although the pier model is made of transparent Perspex and much careful attentions have been given in the fabrication, the junction part (at around x = 1.0 m and 1.05 m) does have some influences on the recorded images and the derived velocity fields. Also the recordings covered only a small portion of the flow field due to the restriction of camera viewing area. One must conduct more runs, keep moving and re-calibrating the PIV system in order to get features in the other regions of interest. This is a common issue of the laboratory model test that cannot be skirted in anyway. In comparisons, the numerical methods like the SPH will not have these limitations as showed below.

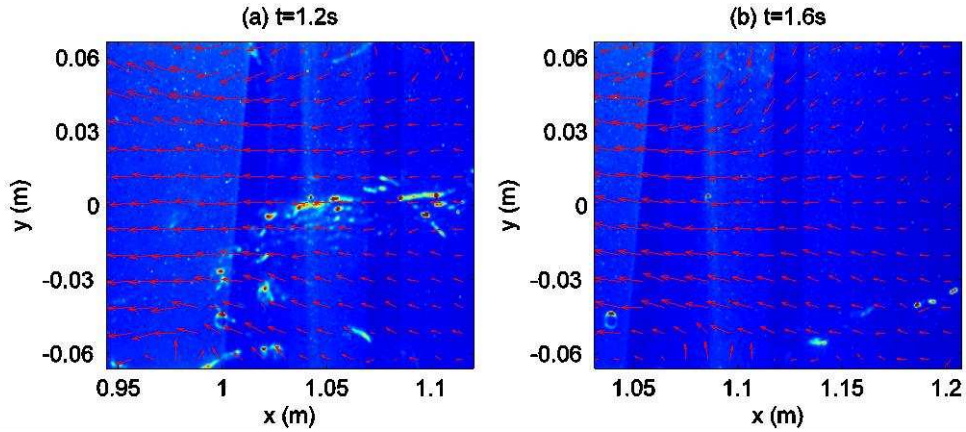

Fig. 13 Experimental images and velocity fields (horizontal)

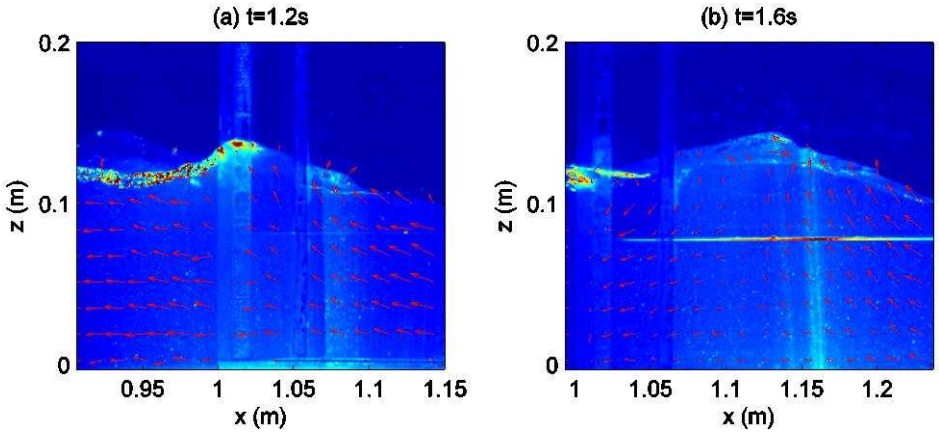

Fig. 14 Experimental images and velocity fields (vertical)

4.2 SPH Simulations and Result Analysis

In the setup of 3D SPH model, the initial particle spacing was still taken as 0.005 m and thus the total number of particles used in the computation was 555,452 for half of the computational domain, including 209,334 fixed boundary particles and 8,118 moving boundary particles to generate the inflow. The time step remained constant at $\Delta t = 2.0 \times 10^{-5}$ s. The employment of the domain separation algorithm has efficiently reduced the CPU time and meanwhile, realistically obtained the 3D flow features.

To validate the numerical results, the computed time histories of the water surface at three different locations, i.e. at the entrance, mid-section and exit of the channel pier restriction, are compared with the experimental measurements in Fig. 15 (a) – (c), respectively. From the figure, we can see that the numerical results generally agreed well with the experimental data in both the bore surface variations and its magnitudes. The disagreement could be attributed to the measurement and numerical errors from different sources. One notable reason could be the result of different setting procedures of the initial bore condition. In the SPH computations, the initial flow depth was first set at 0.1 m and then a flow velocity of 0.3 m/s was imposed to generate the tidal bore. In comparison, the flow velocity was first imposed in the laboratory experiment, and due to the influence of the channel piers the flow depth was not always constant at 0.1 m through the whole channel. Due to this discrepancy in the initial condition, there are larger errors in the computed peak waves at the entrance and exit of the channel constrictions, while a much better agreement was

obtained at the mid-section. The maximum numerical error was around 0.02 m for the former but 0.01 m for the latter.

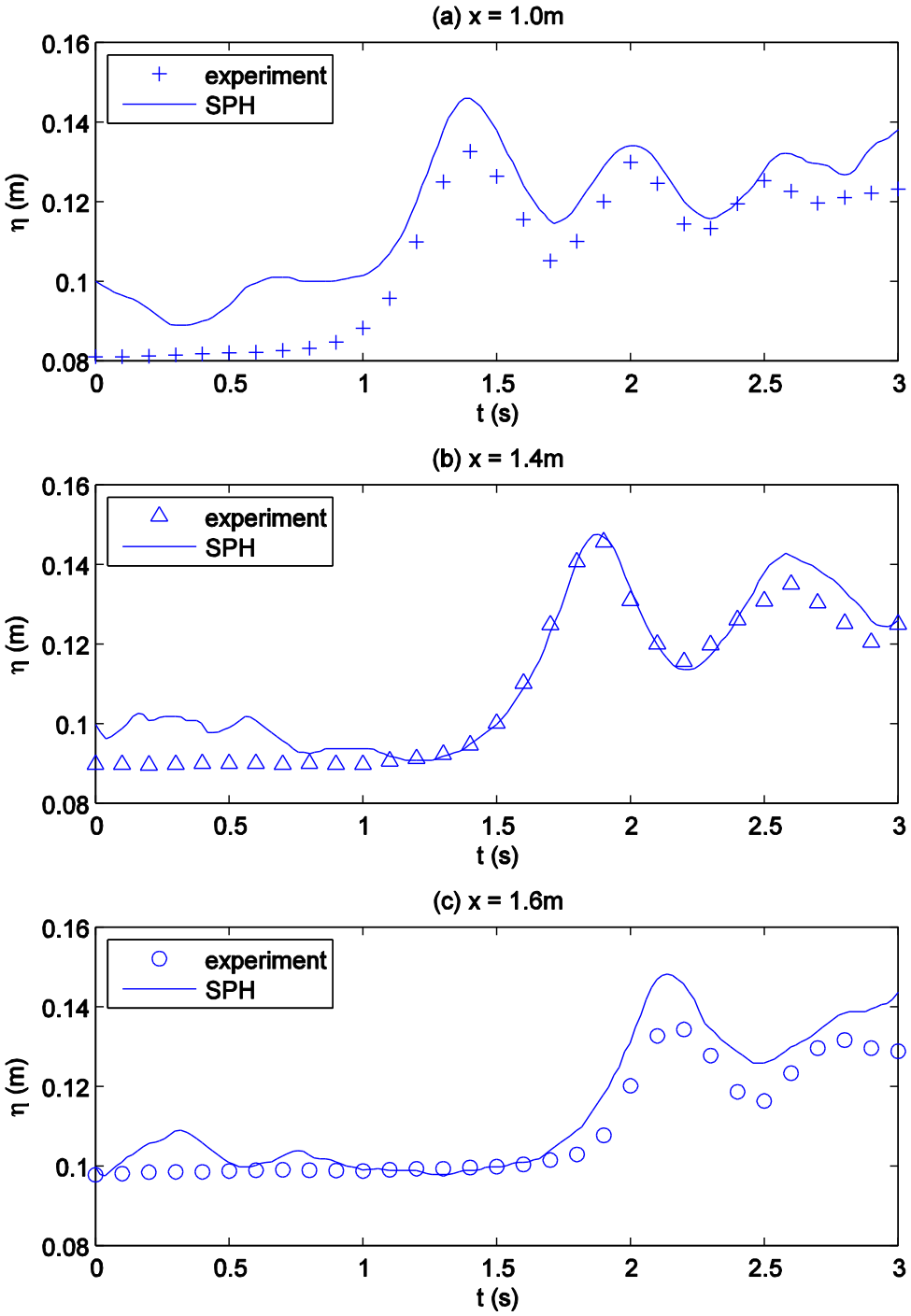

Fig. 15 Computed and measured water surface time histories at three different locations: (a) entrance; (b) mid-section and (c) exit of the channel constrictions

By examining Fig. 15, it shows that the water levels are raised inside the mid-section of the channel constriction. The free surface profiles before and after the constrictions demonstrate the effect of channel contraction and expansion on the tidal bore propagation. This is also consistent with the visual observations, in that some wave reflections happen downstream of the constriction while the channel expansion induces a rapid change in the free surface profiles. Also the data in the mid-section suggest the formation of some secondary waves due to the reflection effect.

To demonstrate the spatial evolution features of the tidal bore propagating across the constricted channel, the simulated 3D particle snapshots at typical timelines are shown in Fig. 16. It shows that the generation and propagation of the bore front are similar to those computed in the previous straight flume before the bore reaches the channel contraction. However, as it is expected the water levels are highly increased when the bore passes through the throat section due to the constriction influence. Also the reflection of bore flow due to the channel piers is clearly visible.

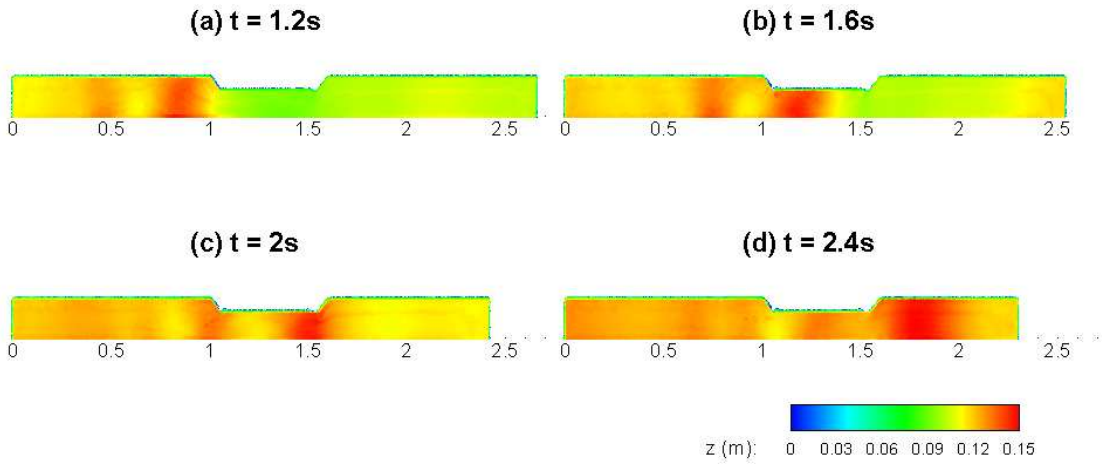

Fig. 16 Particle snapshots of tidal bore passing through channel constrictions

The bore flow horizontal velocity field at plane elevation of z = 0.05 m around the pier sections is shown in Fig. 17, in which a clockwise vortex can be observed at the entrance section of the piers due to the contraction effect. The corresponding vertical velocity field beneath the bore front is given in Fig. 18. Both velocity patterns indicated quite strong flow circulations and turbulence generations, which are not so

obvious in the straight channel case.

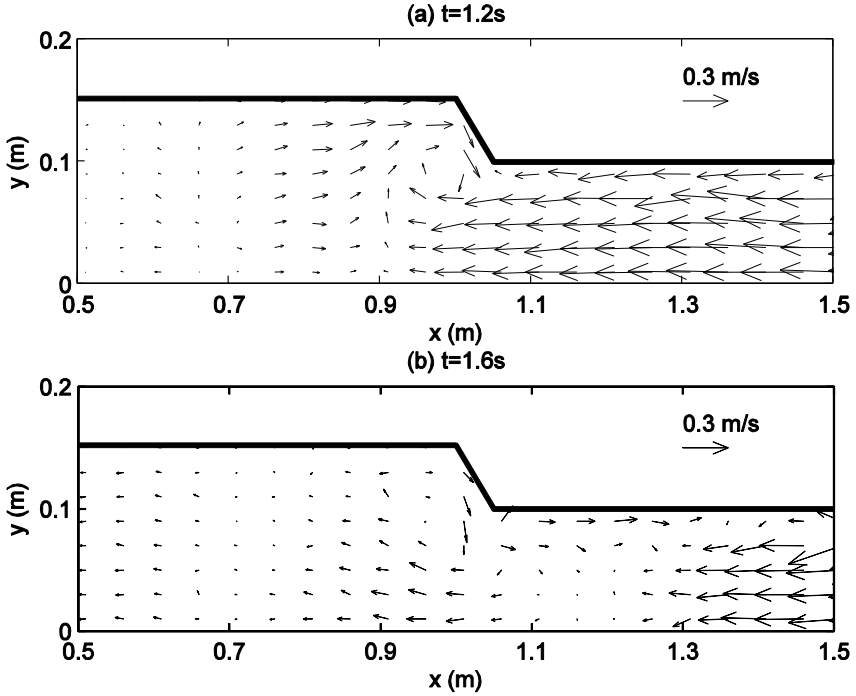

Fig. 17 SPH computed horizontal velocity field (at z = 0.05 m)

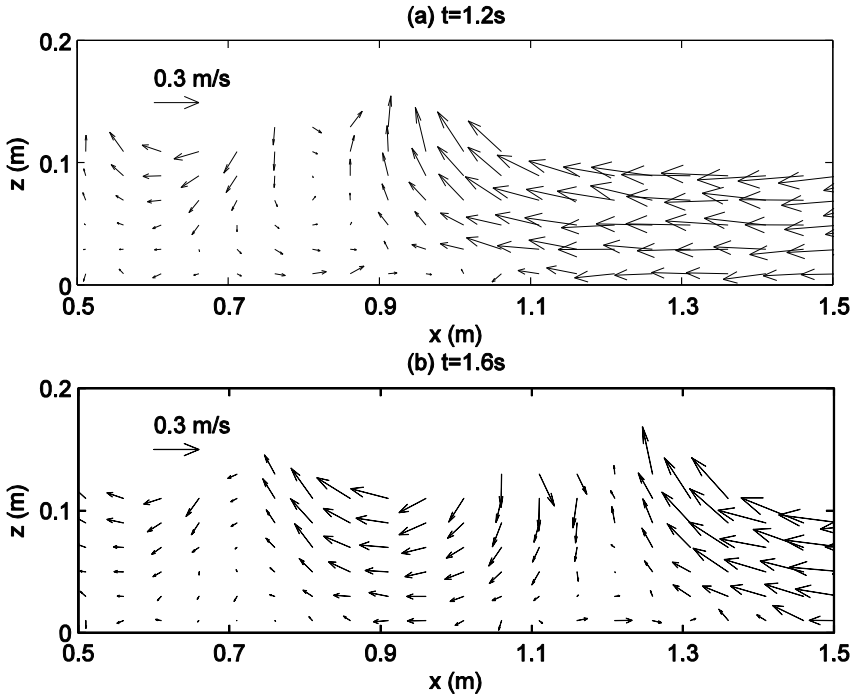

Fig. 18 SPH computed vertical velocity field (at symmetry plane)

By combining the above surface profile and velocity field results, the whole process of undular bore passing through the constricted channel is clearly demonstrated. When the smooth, quasi-periodic shape undular bore approaches the converging section, part of the flow is reflected and propagates back. Around the throat surface area the shock waves are generated, which is an indication of some large turbulent structures near the surface. In the straight channel section, due to the generation of turbulent free surface the flows exhibit strong three-dimensional patterns. The turbulence continues to exist in the wake of sidewall expansion and some distance upstream. Altogether the bore passage is shown to be an energetic turbulent process associated with the strong mixing and being chaotic. Chanson (2011) reported a loss of nearly one third of the potential energy per surface area during this process.

Finally, in order to quantify the influence of channel constriction on the water surface rise, the computed water surfaces with and without the existence of the channel constriction but under the same other flow conditions are shown in Fig. 19 (a) – (c), respectively, for the three measuring locations at the entrance, mid-section and exit of the channel piers. The results have demonstrated that the existence of the channel piers has increased the peak wave levels by around 5 ~ 10% and the nonlinearity and reflection features are also much more visible in that the free surface becomes wavier and less smooth.

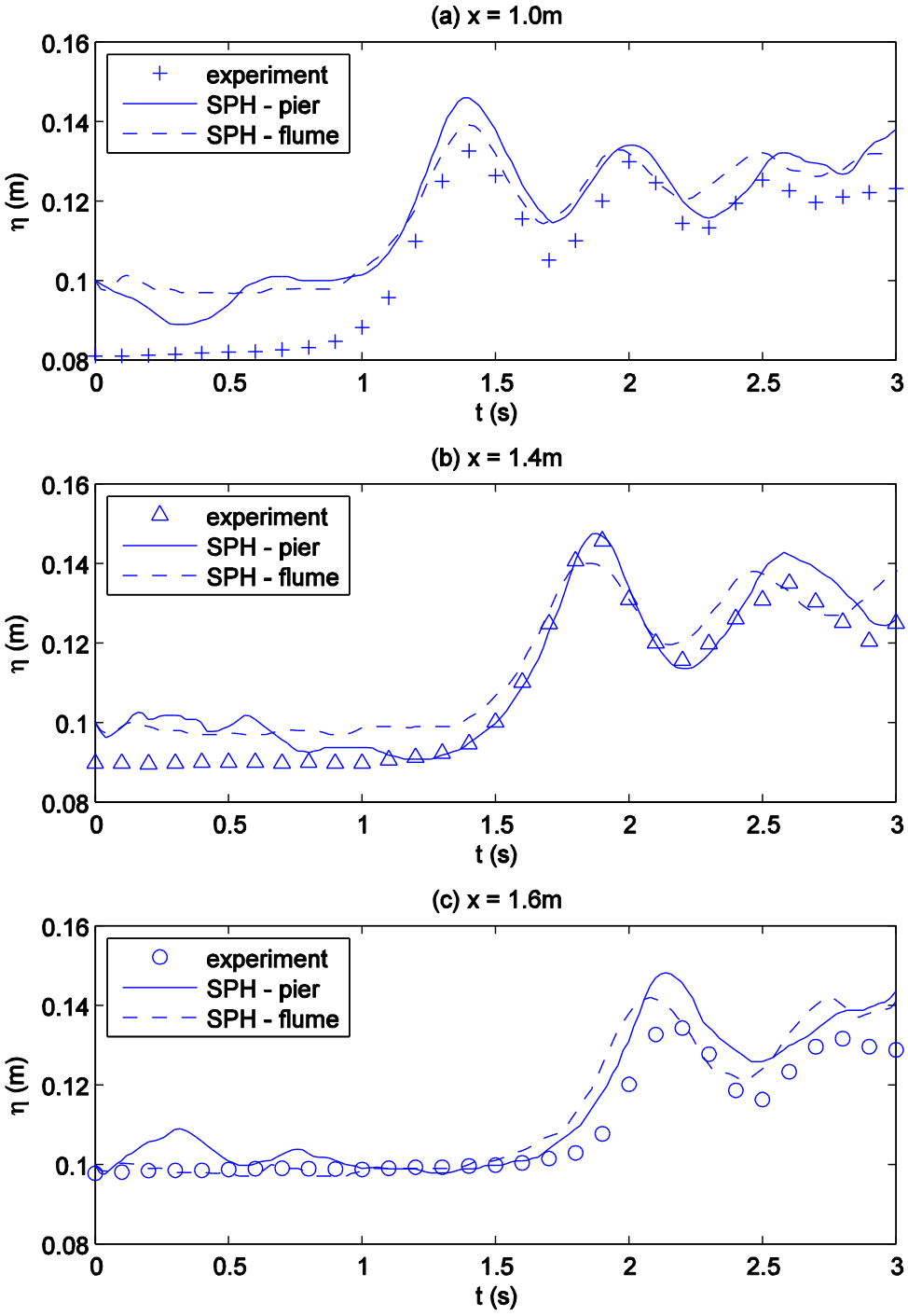

Fig. 19 Comparisons of water surface time histories computed with and without the existence of channel piers at location of (a) entrance; (b) mid-section and (c) exit of channel constriction

5. Conclusions

One 3D SPH model has been applied to simulate the tidal bore process under different inflow and boundary conditions. The undular and breaking bore propagations in a straight unconfined flume, as well as the undular bore propagation in a constricted channel have been analyzed. The computational results demonstrated that the SPH technique reproduced the tidal bore propagations and velocity structures with satisfactory agreement with the experimental data. Meanwhile, the numerical features of SPH could provide more information without the spatial limitations. For the breaking tidal bore and constricted bore flows, the SPH model could reveal distinct 3D flow features, for which the 2D model is incapable of addressing. The comparisons between undular and breaking bore simulations showed substantial turbulence generations and free surface breakings in the latter case, while the comparisons between the simulations with and without the bridge piers have indicated that the existence of such a channel obstacle could amply the bore surface levels and lead to substantial bore reflections near the channel convergence section. Also very strong flow circulations can be generated in this situation. Thus the hydrodynamic features of the tidal bore flow could vary depending on the local situation which should be given adequate attention in the engineering practice.

The contributions of the work lie in the application of mesh-free SPH modeling technique for systematic 3D study of the tidal bore flows in a practical situation, as well as the development of an efficient domain separation algorithm that has significantly reduced the computational load. However, future work will still be needed to study the tidal bore process in more complex bathymetries and geometries.

Acknowledgements

The present work is supported by the National Research Foundation of Singapore through the Competitive Research Programme (No. NRF-CRP5-2009-01) and the NTU-MPA Maritime Research Centre. Songdong Shao acknowledges the support of

the Major State Basic Research Development Program (973 program) of China (No. 2013CB036402) and the Open Fund from the State Key Laboratory of Hydraulics and Mountain River Engineering, Sichuan University, China (No. SKLH-OF-1103).

References

Behera, M.R., Murali, K., Sundar, V., 2011. Effect of the tidal currents at the amphidromes on the characteristics of an N-wave-type tsunami. Proceedings of the Institution of Mechanical Engineers Part M - Journal of Engineering for the Maritime Environment 225(M1), 43-59.

Benet, F., Cunge, J.A., 1971. Analysis of experiments on secondary undulations caused by surge waves in trapezoidal channels. Journal of Hydraulic Research 9(1), 11-33.

Bonet, J., Lok, T.S.L., 1999. Variational and momentum preservation aspects of Smooth Particle Hydrodynamic formulations. Computer Methods in Applied Mechanics and Engineering 180, 97-115.

Chanson, H., 2011. Undular tidal bores: effect of channel constriction and bridge piers. Environmental Fluid Mechanics 11, 385-404.

Chen, W., Panchang, V., Demirbilek, Z. 2005. On the modeling of wave-current interaction using the elliptic mild-slope wave equation. Ocean Engineering 32(17-18), 2135-2164.

Crespo, A.J.C., Gomez-Gesteira, M., Dalrymple, R.A., 2007. Boundary conditions generated by dynamic particles in SPH methods. Computers, Materials and Continua 5(3), 173-184.

Cummins, S.J., Rudman, M., 1999. An SPH projection method. Journal of Computational Physics 152(2), 584-607.

Farahani, R.J., Dalrymple, R.A., Herault, A., Bilotta, G., 2014. Three-dimensional SPH modeling of a bar/rip channel system. Journal of Waterway, Port, Coastal and Ocean Engineering, 140(1), 82-99.

Furuyama, S., Chanson, H., 2010. A numerical simulation of a tidal bore flow. Coastal Engineering Journal 52(3), 215-234.

Gingold, R.A., Monaghan, J.J., 1977. Smoothed particle hydrodynamics: theory and application to non-spherical stars. Monthly Notices of the Royal Astronomical Society 181, 375-389.

Gómez-Gesteira, M., Rogers, B.D., Crespo, A.J.C., Dalrymple, R.A., Narayanaswamy, M., Dominguez, J.M., 2012. SPHysics - development of a free-surface fluid solver - part 1: theory and formulations. Computers & Geosciences, doi:10.1016/j.cageo.2012.02.029, http://www.sphysics.org.

Gotoh, H., Shibahara, T., Sakai, T., 2001. Sub-Particle-Scale turbulence model for the MPS method – Lagrangian flow model for hydraulic engineering. Computational Fluid Dynamics Journal 9(4), 339-347.

Hornung, H.G., Willert, C., Turner, S., 1995. The flow field downstream of a hydraulic jump. Journal of Fluid Mechanics 287, 299-316.

Hirt, C.W., Nichols, B.D., 1981. Volume of fluid (VOF) method for the dynamics of free boundaries. Journal of Computational Physics 39, 201-225.

Khezri, N., Chanson, H., 2012. Undular and breaking tidal bores on fixed and movable gravel beds. Journal of Hydraulic Research 50(4), 353-363.

Landrini, M., Colagrossi, A., Greco, M., Tulin, M.P., 2007. Gridless simulations of splashing processes and near-shore bore propagations. Journal of Fluid Mechanics 591, 183-213.

Lastiwka, M, Basa, M., Quinlan, N.J., 2009. Permeable and non-reflecting boundary conditions in SPH. International Journal for Numerical Methods in Fluids 61, 709-724.

Li, J., Liu, H., Tan S.K., 2010. Lagrangian modeling of tidal bores passing through bridge piers. Journal of Hydrodynamics, Ser. B 22(5), 513-519.

Liang, D., Falconer, R.A., Lin, B., 2006. Improved numerical modelling of estuarine flows. Proceedings of the Institution of Civil Engineers – Maritime Engineering 159(1), 25-35.

Lin, P.Z., Liu, P.L.F., 1998. Turbulence transport, vorticity dynamics, and solute mixing under plunging breaking waves in surf zone. Journal of Geophysical Research – Ocean 103(C8), 15677-15694.

Liu, G.R., Liu, M.B., 2003. Smoothed Particle Hydrodynamics: A Meshfree Particle Method. World Scientific, 3rd printing.

Liu, H., Tan, S. K., Li, J., Wang, X., 2010. Three dimensional simulation of bore flow using SPH. 29th International Conference on Ocean, Offshore and Arctic Engineering (OMAE 2010), Shanghai, China.

Lucy, L.B., 1977. A numerical approach to the testing of the fission hypothesis. The Astronomical Journal 82, 1013-1024.

Madsen, P.A., Simonsen, H.J., Pan, C.H., 2005. Numerical simulation of tidal bores and hydraulic jumps. Coastal Engineering 52, 409-433.

Monaghan, J.J., Lattanzio, J.C., 1985. A refined method for astrophysical problems. Astronomy and Astrophysics 149(1), 135-143.

Monaghan, J.J., 1992. Smoothed particle hydrodynamics. Annual Review of Astronomy and Astrophysics 30, 543-574.

Monaghan, J.J., 1994. Simulating free surface flows with SPH. Journal of Computational Physics 110, 399-406.

Morrison, G.M., 2008. Numerical Modelling of Tidal Bore Using a Moving Mesh. MSc dissertation, Department of Mathematics, University of Reading, UK, 2008.

Pan, C.H., Lin, B.Y., Mao X.Z., 2007. Case study: numerical modeling of the tidal bore on the Qiantang river, China. Journal of Hydraulic Engineering 133(2), 130-138.

Pan, C.H., Huang, W., 2010. Numerical modeling of suspended sediment transport affected by tidal bore in Qiantang estuary. Journal of Coastal Research 26(6), 1123-1132.

Shao, S.D., Lo, E.Y.M., 2003. Incompressible SPH method for simulating Newtonian and non-Newtonian flows with a free surface. Advances in Water Resources 26, 787-800.

Simpson, J.H., Fisher, N.R., Wiles, P., 2004. Reynolds stress and TKE production in an estuary with a tidal bore. Estuarine, Coastal and Shelf Science 60(4), 619-627.

St-Germain, P., Nistor, I., Townsend, R., Shibayama, T., 2014. Smoothed-particle hydrodynamics numerical modeling of structures impacted by tsunami bores. Journal of Waterway, Port, Coastal, Ocean Engineering, 140(1), 66–81.

Su, M.D., Xu, X., Zhu, J.L., Hon, Y.C., 2001. Numerical simulation of tidal bore in Hangzhou Gulf and Qiantangjiang. International Journal for Numerical Methods

in Fluids 36(2), 205-247.

Treske, A., 1994. Undular bores (favre-waves) in open channels – experimental studies. Journal of Hydraulic Research 32(3), 355-370.

Xie, J., Nistor, I., Murty, T., 2012. A corrected 3-D SPH method for breaking tsunami wave modelling. Nat Hazards 60, 81–100.

Zheng, J., Mase, H., Demirbilek, Z., 2008. Implementation and evaluation of alternative wave breaking formulas in a coastal spectral wave model. Ocean Engineering 35(11-12), 1090-1101.

Zhu, S., Cheng, X., 2008. Test and analyses of a new double-arch steel gate under cyclic loads. Journal of Constructional Steel Research 64(4), 454-464.